IOPscience iopscience.iop.org

Home Search Collections Journals About Contact us My IOPscience

Low energy focused ion beam milling of silicon and germanium nanostructures

This article has been downloaded from IOPscience. Please scroll down to see the full text article.

2011 Nanotechnology 22 105304

(http://iopscience.iop.org/0957-4484/22/10/105304)

View the table of contents for this issue, or go to the journal homepage for more

Download details:
IP Address: 130.209.6.41
The article was downloaded on 05/04/2012 at 17:54

Please note that terms and conditions apply.

Nanotechnology **22** (2011) 105304 (8pp) doi:10.1088/0957-4484/22/10/105304

Low energy focused ion beam milling of silicon and germanium nanostructures

Miroslav Kolíbal[1], Tomáš Matlocha[1], Tomáš Vystavěl[2] and Tomáš Šikola[1]

[1] Institute of Physical Engineering, Brno University of Technology, Technická 2, 61669 Brno, Czech Republic
[2] FEI Company, Podnikatelská 6, 61200 Brno, Czech Republic

E-mail: kolibal.m@fme.vutbr.cz

Received 13 September 2010, in final form 17 December 2010
Published 2 February 2011
Online at stacks.iop.org/Nano/22/105304

Abstract
In this paper focused ion beam milling of very shallow nanostructures in silicon and germanium by low energy Ga^+ ions is studied with respect to ion beam and scanning parameters. It has been found that, using low energy ions, many scanning artefacts can be avoided and, additionally, some physical effects (e.g. redeposition and ion channelling) are significantly suppressed. The structures milled with low energy ions suffer less subsurface ion beam damage (amorphization, formation of voids) and are thus more suitable for selected applications in nanotechnology.

(Some figures in this article are in colour only in the electronic version)

1. Introduction

Focused ion beam (FIB) machines are now routinely used in sample preparation for transmission electron microscopy (TEM), optical lithography mask repairs and tomography. Apart from these major areas of use, FIB has also been utilized in newly developed patterning techniques for fabrication of nanocontact print masters [1, 2] or etching masks for photonic crystals [3] and, thus, seems to remain a prominent technology in this field. The advantage of a dual-beam instrument (with both electron and ion beams available) is the ability to localize a desired place on a sample and to remove or add material with a high precision without any resist layer or etching mask. The dual-beam systems therefore represent an ideal platform for repairs and, also, fabrication/prototyping of individual devices [4], as demonstrated by the preparation of photonic crystal slabs [5], polymer light-emitting diodes [6] or by manufacturing field emitter structures on the top of an SPM tip [7]. There were also attempts to move towards a larger scale fabrication. The growth of spatially ordered nanostructures was achieved on FIB milled holes via surface energy reduction [8] or on FIB-intended nucleation sites [9–12]. Although doubts still exist on FIB usability at a larger scale due to a low throughput, recently a large scale patterning with multiple write-fields using a conventional dual-beam set-up has been demonstrated [13].

Obviously, all these applications require full control over the fabrication of various structural shapes even at the nanoscale. There have been discussions on the influence of ion beam parameters (beam current, scanning strategy, etc) and physical effects (implantation, sputtering, amorphization, etc) on the shape of milled structures. However, there are still some issues remaining. In this paper, FIB milling of silicon and germanium nanostructures is discussed with respect to the most important processing parameters. It is shown and explained that many physical effects become minor and the milling process simpler by reducing ion energy to 5 keV. Until now low energy ions have been almost exclusively used for final polishing of TEM lamellas (2 keV), making high-resolution imaging in TEM possible [14, 15]. We show that the milling at nanoscale with low energy ions is profitable in many other applications. For instance, improved shapes of the structures milled in germanium have been obtained with low energy ions, which is unachievable at higher energies due to the formation of nanopores and large protrusions under ion bombardment.

2. Experimental methods

Both silicon ((111) and (100) orientation, P-doped, 0.01 Ω cm, ON Semi) and germanium wafers ((100), Ga-doped, 0.01–0.04 Ω cm, Si-Mat) were cut into smaller pieces (10×10 mm^2)

 © 2011 IOP Publishing Ltd Printed in the UK & the USA

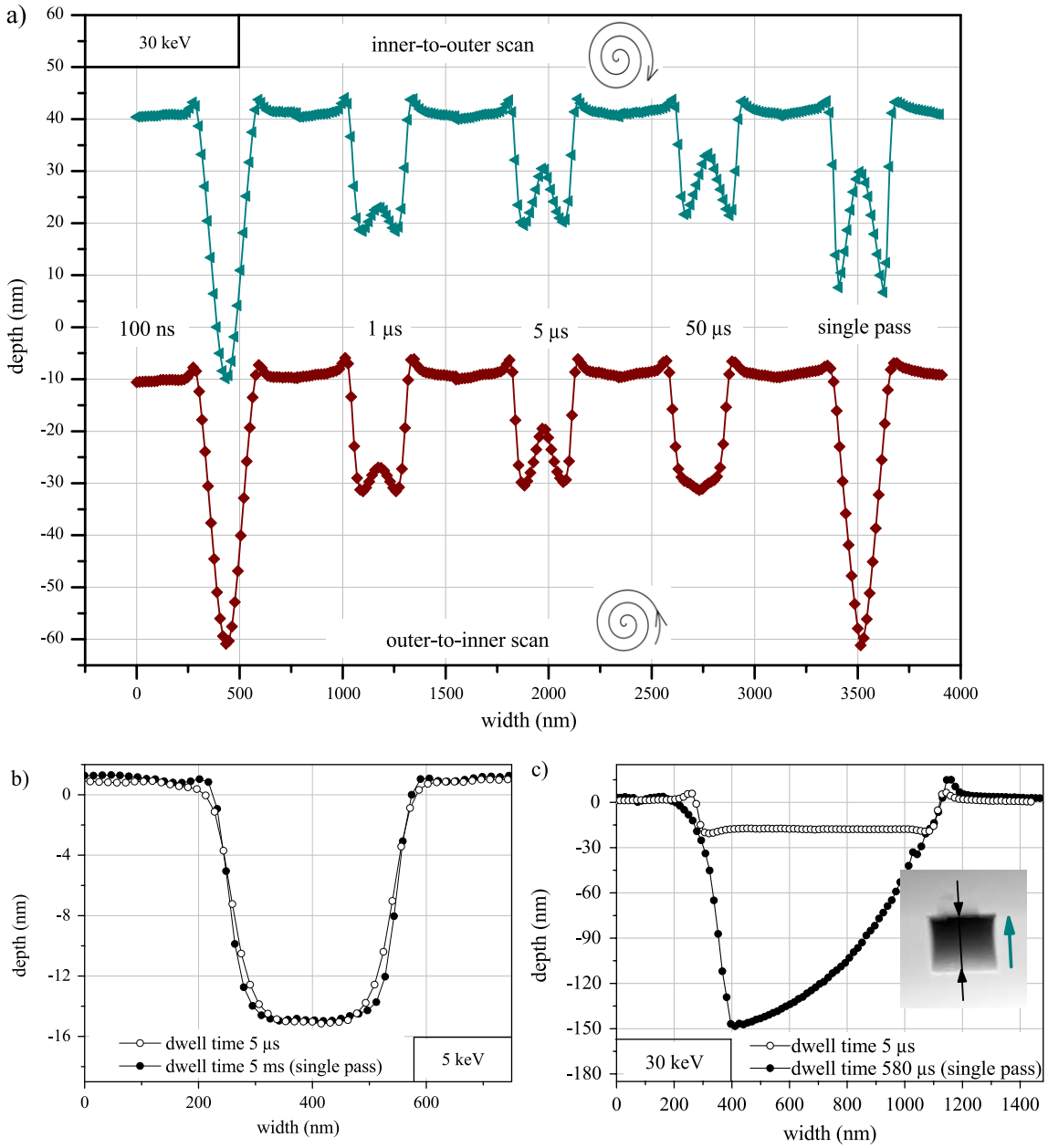

Figure 1. (a), (b) AFM profiles of circular holes 300 nm in diameter milled into an Si(111) silicon wafer by (a) 30 keV and (b) 5 keV Ga^+ ions. Spiral scanning strategy was used; dwell times as well as scanning directions are marked in the image. Only two AFM profiles are presented in (b), since for the dwell times used (1 μs–5 ms) and scanning directions the obtained hole profiles were the same. The effect of a large dwell time is demonstrated in (c), where an AFM profile of a rectangular hole milled by a single ion beam pass (580 μs dwell time) of a 30 keV ion beam is shown. The scanning direction was bottom to top (indicated by the large green arrow in the inset). For comparison, an AFM profile of a hole milled using the same ion fluence but a smaller dwell time of 5 μs and a larger number of passes (102) is shown. The inset shows an AFM image of the single-pass milled rectangular hole, where the smaller black arrows indicate the profile plane.

and loaded into the FIB-equipped sample chamber. Most of the experiments were done on an FEI Quanta 3D FEG Dual Beam system (silicon milling experiments presented in figure 1 and germanium milling). To avoid any hardware-related artefacts, reference milling experiments were performed on an FEI Helios Nanolab Dual Beam system giving similar results (not presented here). Additionally, cross-sectioning of the milled structures (presented in figure 2) was done on this system. After sample insertion the microscope chamber was evacuated to a pressure better than 2×10^{-4} Pa, being the prerequisite for low energy ion beam fabrication. At higher pressures, an additional ion scattering from residual gas atoms significantly broadens the ion beam at low energies, thus resulting in deterioration of the achievable resolution.

Since the results obtained on crystallographically different silicon substrates do not vary significantly, only structures milled into Si(111) will be presented in this paper.

In the experiments Ga^+ ions having two distinct energies (30 and 5 keV) were used. To keep the probe size small, very low currents (<30 pA) were used. Circular and rectangular

Table 1. Ion beam parameters for both FIB systems including several SRIM calculated data for Si and Ge targets.

Ion energy (keV)	Current (pA)	Spot size (nm)	Ion range (nm)	Sputtering yield	Vacancies/ion
30	1.5/24[a]	7/13[a]	28/18.2[b]	2.2/4.8[b]	745/1078[b]
5	4/7[a]	36/31[a]	8.5/5.4[b]	1.3/3.4[b]	144/189[b]

[a] Data for Helios Nanolab. [b] Calculated for Ge target.

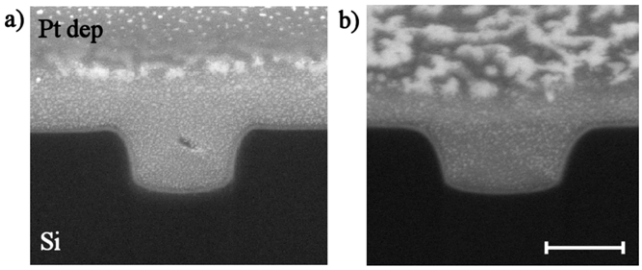

Figure 2. Cross-sectioned circular holes (300 nm diameter) milled by (a) 30 keV and (b) 5 keV ion beam into silicon. The scale bar is 200 nm and the image is tilted by 38°. The dimensions of the holes are presented in table 3.

objects having lateral dimensions 300 nm and 1 μm, and depths ∼20 and ∼160 nm were used as test structures. The fluence necessary to mill the structures of a certain depth was determined by comparing the depth values set in the FIB control software with those obtained experimentally by AFM. The parameters which can be changed by an operator include dwell time, scanning strategy and beam overlap. The dwell time is a time interval that the beam spends on a single milling spot (further called the milling point). Note that the dimension of the milling point (spot size) is a theoretically calculated value (FWHM of the Gaussian distribution) and depends on the beam energy and current. Circular shapes are patterned by a spiral scanning with two strategies: outer to an inner diameter (OI) or inner to an outer diameter (IO). The scanning strategy for the rectangular shapes includes bottom-to-top and left-to-right raster or serpentine scans and their reversed variations. The overlap is controlled by a parameter called the pitch, which is the distance between the centres of two consecutive milling points. The overlap is usually varied in the range from 50% for milling (pitch equal to one half the calculated spot size) to −50% for deposition (pitch equal to three halves the calculated spot size). In this work only the 50% overlap was used. Since the real spot size and the theoretically calculated one may differ (the beam defining apertures degrade in time due to sputtering), this value can be misleading and should be used only in a relative, not absolute, manner. The most important ion beam parameters for both FIB systems used together with several SRIM calculated values are presented in table 1.

Fabricated nanostructures were analysed *ex situ* by Ntegra Prima AFM, preferentially using the same piece of a cantilever (NT-MDT CSG-11, tip curvature radius <10 nm) to avoid tip-induced scanning artefacts. Note that the data were not deconvoluted with respect to the tip shape, since the structures prepared were shallow (<20 nm) and large enough in comparison with the tip radius. The only parameter distorted to some extent in the measurements with such a tip is the inclination of the milled structure wall. Therefore, to get more precise information on the shape of the fabricated structures a cross-sectioning by FIB (FEI Helios Nanolab) was done. First, the corresponding sample areas were Pt-coated *in situ* by e-beam deposition to protect the sample from milling outside the desired area, which might affect the milled shapes and result in misinterpretation of the results. The profiles of the fabricated structures were afterwards analysed using a standardized FEI cross-sectional technique.

Computer simulations of ion scattering and other ion-induced effects in the sample were performed by the SRIM code [16].

3. Silicon milling

Figures 1(a) and (b) show the AFM measured profiles of circular holes (300 nm in diameter, ∼20 nm in depth) milled with 30 keV (figure 1(a)) and 5 keV (figure 1(b)) ion beams, respectively. Milling was done using both IO and OI scanning strategies and several dwell times, ranging from a very short value of 100 ns till 580 μs or 5 ms. Both upper limits represent a single-pass milling (each milling point is exposed only once) for 30 keV and 5 keV, respectively. The patterning parameters as well as dimensions of milled structures are summed in table 2(a) and (b). Note that the length scale in figure 1 is different for x and y axes and thus the shape of the hole bottom is emphasized. The hole bottom shape is critical for mask repair and preparation techniques and also plays a crucial role in the nanodot's positioning via the energy reduction growth mechanism. Apparently, the hole bottom is far from being flat for most of the structures prepared by 30 keV ions. For 5 keV ions only two AFM profiles are presented, because the experiments gave less complex results with respect to the desired flat bottom. Irrespective of the scanning strategy and dwell time (except the shortest 100 ns dwell time, which is not appropriate for patterning, as described further in the text), the holes milled with 5 keV ions were of an identical shape (even in the case of single-pass milling, as presented in figure 1(b)). The upper diameter of the holes was ∼305 nm and ∼380 nm for 30 keV and 5 keV ions, respectively. The diameters were different from the above quoted values if very short (100 ns) or long (single-pass milling) dwell times were used.

To get information on the milled pattern profiles unaffected by the shape of an AFM tip, additional circular holes were fabricated and cross-sectioned by FIB (FEI Helios Nanolab) and imaged by SEM (figure 2). The nominal depth of the holes was increased to 160 nm using a milling current higher than in previous experiments, 24 pA for 30 keV and 7 pA for 5 keV. Other parameters (scanning strategy, dwell time) were chosen with respect to achieving flat bottoms. The applied ion beam parameters are summarized in table 1, while

Table 2. Detailed patterning parameters and dimensions of features presented in figure 1. (a) Circular holes, 30 keV ions, 1.5 pA current, ∼5800 milling points per feature. (b) Circular holes, 5 keV ions, 4 pA current, ∼260 milling points. (c) Rectangular holes, 30 keV, 1.5 pA current, ∼70 000 milling points per feature.

			IO scanning direction		OI scanning direction	
Dwell time (μs)	Passes	Loop time (ms)	Upper diameter (nm)	Depth (nm)	Upper diameter (nm)	Depth (nm)
(a)						
0.1	5717	0.583	285	51	282	51
1	572	5.8	305	23	299	22
5	114	29.1	306	22	306	21
50	11	290.6	318	21	298	23
580	1	3370	314	35	289	53
(b)						
0.1	48 689	0.026	412	13	389	13
1	5221	0.249	383	15	383	15
5	1083	1.3	383	16	383	16
500	10	124	388	16	388	16
5000	1	1240	370	16	370	16
(c)						
Dwell time (μs)	Passes	Loop time (ms)	Side (nm)	Depth (nm)		
5	101	372.6	848	19.2		
580	1	3.8×10^4	918	149		

Table 3. Dimensions of the features presented in figure 2.

Ion energy (keV)	Dwell time (μs)	Passes	Loop time (ms)	Upper diameter (nm)	Bottom diameter (nm)	Depth (nm)	Sidewall angle (deg)
30	1	931	1.8	320	237	162	14.3
5	5	3656	1.5	351	285	175	21

the other fabrication parameters are in table 3. It is apparent from the figure that the absence of the rim around the hole milled with 5 keV ions (figure 2(b)) is caused not only by a smaller contribution of surface swelling (see section 3.3), but also by additional sputtering due to extended beam tails. In the case of 30 keV ions this additional hole-opening effect was reported to become significant for aspect ratios starting from 1:4 on [17]. For 5 keV ions this critical aspect ratio is 1:10 or even less. The wall inclination angle is higher for structures milled with low energy ions (21° in comparison with 14.5°). Hence, due to the extended beam tails the smallest possible structure to be milled with a 5 keV ion beam is larger than the one done by a 30 keV ion beam and critically depends on the aspect ratio. The milling resolution can be significantly enhanced using a protective layer as reported in [18].

The following subsections will focus on the physical principles responsible for different shapes prepared by ion milling under various parameters.

3.1. Redeposition and sputtering on an inclined surface

A very different shape from the desired one is obtained using the shortest dwell time (100 ns). At 30 keV, instead of 20 nm a 50 nm deep V-shaped hole was fabricated (figure 1(a)). Similarly, a very unpredictable shape was obtained by using 5 keV ions as well (not presented here). The reason for using very short dwell times and more beam passes was to avoid the redeposition [19] (redeposited material is immediately milled away in the next pass), a physical mechanism referred to causing the unusual milled shapes. However, the beam blanking time (∼100 ns) is comparable to these short dwell times, which results in improperly defined beam scanning over the exposed area and, therefore, in unpredictable structure shapes. Hence, these hardware-limited effects are very important for choosing the right patterning parameters.

Obviously, the shortest dwell times are not convenient for patterning. However, by increasing this parameter to 1 μs the scanning artefacts become negligible and almost perfect holes are fabricated (see figure 1(a)), independent of the scanning direction. The small protrusion in the centre of the hole is the result of redeposition [20]. This is proven by the fact that, if the dwell time is increased, the protrusion height increases while the hole depth remains the same (figure 1(a)). Note that only the atoms sputtered from the walls can be redeposited in the centre, since the trajectories of the sputtered atoms are straight and the redeposition is a simple geometric effect. Another explanation of the W shape of the hole could be so-called self-focusing [20], which is an additional sputtering of the hole edges due to ions scattered from the walls. Comments on this effect will be given later on, but if it was the case, the hole should be deeper. If the dwell time is increased to 50 μs for

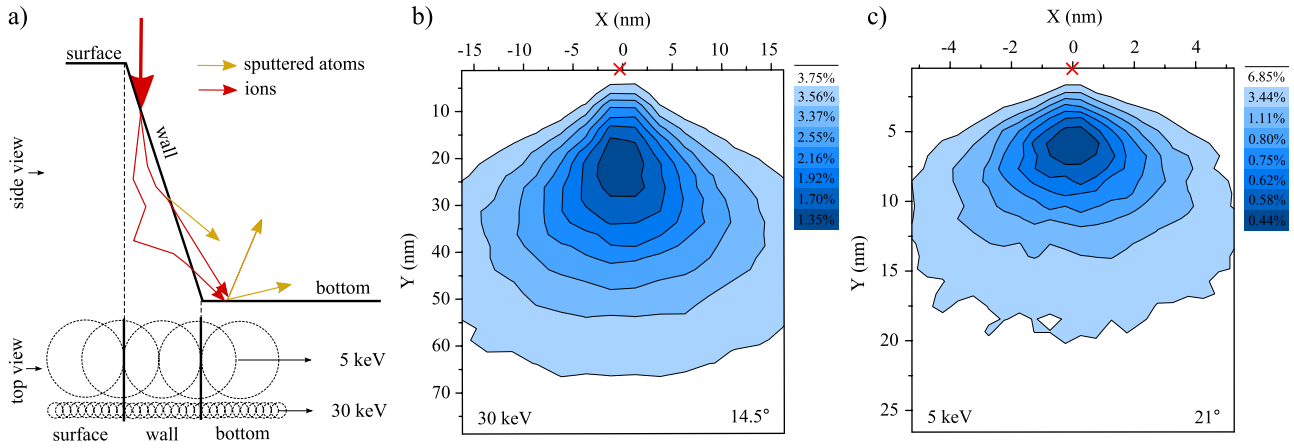

Figure 3. Computer simulations of primary ions scattered from an inclined wall. (a) Ion beam impinges onto a wall inclined with respect to the surface normal. Dark grey lines (red in electronic version) schematically represent Ga^+ ion trajectories, light grey lines (yellow in electronic version) the sputtered atoms. Note that only atoms sputtered from the walls can be redeposited on the bottom. The dashed circles below show the milling points (represented by the spot size, viewed from the top) for 5 and 30 keV ions. (b), (c) Surface maps of scattered ions corresponding to the wall in (a), calculated by SRIM for (b) 30 keV ions and (c) 5 keV ions. The colours in the surface map indicate a percentage of primary ions emerging after scattering from the particular wall sites; the beam impact site is marked with the red cross. Wall inclination angles are indicated in the image and correspond to the values measured on cross-sectioned FIB milled holes.

30 keV ions, the scanning direction becomes important again. While the IO scanning direction leads to an enhanced central protrusion, OI scanning reverses the process and the bottom gets deeper. In the case of single-pass milling one can obtain either the almost 40 nm deep W-shaped hole with an upper diameter of 314 or the 50 nm deep V-shaped hole with an upper diameter of 289 nm, depending on the scanning direction (figure 1(a)). The change in the hole diameter in comparison to those milled using shorter dwell times can be easily explained by redeposition. If the beam starts at the outer diameter and moves to the centre along the spiral trajectory, the redeposition of the sputtered material onto the walls finally results in a smaller hole diameter. If the opposite scanning direction is used the redeposition onto the walls is effectively suppressed.

However, these V- and W-shaped holes are deeper than expected. Therefore their formation cannot be explained by redeposition only [20, 21]. Here a third important effect in ion sputtering plays a major role—enhanced sputtering rate on inclined surfaces. Sputtering yield increases with an incident angle and shows a maximum around 70°–80° [22]. In the single-pass milling procedure, the position of the first milling point defines the final shape of the structure. If the milling starts in the middle, the W shape is obtained since every consecutive exposure results in a deeper structure due to higher sputtering yields at the locally inclined surfaces (beam overlap is 50% and the beam has extended tails). If the scan starts at the outer diameter the situation is reversed. This effect is quite strong for 30 keV ions and significantly overruns the redeposition for dwell times slightly below 50 μs and higher ones. Such an effect is also illustrated in figure 1(c), where two profiles (milled by 30 keV ions with a single pass and multiple passes with 5 μs dwell time) of a rectangular hole are compared. The redeposition is not the major mechanism here. It is intriguing that the hole profiles milled with 5 keV ions look almost similar, independently of the scanning direction and the effect of locally inclined surfaces is suppressed.

Now the question arises: why the structures milled by 5 keV ions using different dwell times are nearly identical? All the holes have flat bottoms, including single-pass milled ones. First, the low energy ions have a lower sputtering efficiency and, more importantly, the beam is significantly broader (see the calculated beam spot size and sputtering yield/ion in table 1). Therefore, there is a smaller number of ions per each scanning loop at low energies and more beam passes are necessary to sputter the same amount of material, resulting in a more uniform milling. Hence, the dwell time is not an appropriate parameter for optimization of the milling process. A simple calculation gives the following results: for 30 keV ion beam (beam current 1.5 pA) and dwell time 100 ns the ion fluence is 2.4×10^{12} ions cm^{-2}, while at 5 keV (current 4 pA) this fluence is only 2.4×10^{11} ions cm^{-2}. Such a low ion fluence typical for lower energies cannot be reached at 30 keV (because both dwell time and current cannot be decreased further), which represents an additional advantage of low energy ion patterning.

3.2. Ion scattering from the walls

From the previous discussion it is clear that the optimum patterning conditions for most applications lay between the extremely short dwell time and the single-pass milling. The amount of redeposition increases with increasing dwell time, being significantly lower at 5 keV due to smaller current density of the beam. A second important effect is the ion scattering from the walls, sometimes referred to as self-focusing [23–25]. The primary heavy Ga ions can be scattered forward from the walls of milled structures (or deposited ones [26, 27]), thus increasing the sputtering rate at their bottom corners. This effect was indicated in the papers as being responsible for the W shape of the hole. Here it is shown that, if the pattern dimensions remain at the nanoscale, the ion scattering effect is minor and the central hillock (if present)

is mainly due to redeposition (except single-pass milling, as discussed above). The schematic in figure 3(a) shows the ion beam impinging onto a milled structure wall inclined from the surface normal. The red lines are the primary ion trajectories, while yellow lines show possible sputtered atoms. The dashed circles below show the milling points (represented by the spot size) for 5 and 30 keV ions. In figure 3(b) a surface map of forward scattered ions (30 keV) corresponding to the wall in figure 3(a) is shown. A wall inclination angle of 14.5° was determined from the cross section of a 160 nm deep hole with the 300 nm diameter (presented in figure 2). The colours in the surface map indicate a percentage of primary ions emerging after scattering from the particular wall sites; the beam impact site is marked with a red cross. To keep the simulation simple the beam spot was infinitely small. The most important feature is that the ions are not scattered out of the wall surface from the impact position, but travel a relatively long distance in the sample before leaving its surface with less energy. For a 20 nm deep hole milled with 30 keV ions and an impact site at the top edge, only 3% of ions are scattered from the surface into the free space; the rest are trapped inside the sample. For much deeper holes the larger amount of primary ions is scattered forward (20% for the hole deeper than 70 nm) and impinges on the hole bottom. This simulation explains why the ion scattering effects become efficient in determining the hole shape only for sufficiently deep holes. However, in our experiment we have not observed any additional sputtering close to the bottom edge even for the holes 160 nm deep. The effect becomes evident for very deep structures only (deeper than 1 μm, as reported in [24]).

For smaller wall inclination angles the number of scattered particles dramatically increases. The smallest value reported so far is 5.5° (using a protective layer which suppresses additional sputtering due to beam tails [18]), which gives 38% of primary ions being scattered from the walls. However, note that, if the inclination angle is smaller, the number of primary ions hitting the wall decreases (the projection of the wall onto the surface plane gets smaller and, hence, it contains less milling points). Therefore, the total amount of ions scattered from the walls does not generally increase with smaller inclination angles.

The ion range (and, consequently, the amount of scattered ions) scales with ion energy. In figure 3(c) the same type of surface map is shown for 5 keV ions. Although the number of scattered ions increases (8.5% at 20 nm below the impact place compared to 3% at 30 kV), the enhanced sputtering due to ion focusing effects is again not visible in the hole profiles (figure 1(b)). As the beam size for 5 keV ions is larger than for 30 keV the beam possesses lower current density. To give the evidence of an amount of sputtered atoms from the hole bottom a simple calculation will be made. The number of atoms sputtered from the hole bottom per loop N can be calculated as

$$N = \frac{It}{e}\frac{S}{S^{\mathrm{s}}}cXY_{\mathrm{s}} \qquad (1)$$

where I is the ion current, t is the dwell time, e is the elementary charge, S is the area of the wall projection onto the surface, S^s is the area of a beam spot, c is the parameter dependent on the overlap value (1 for 0% overlap, 4 for 50%),

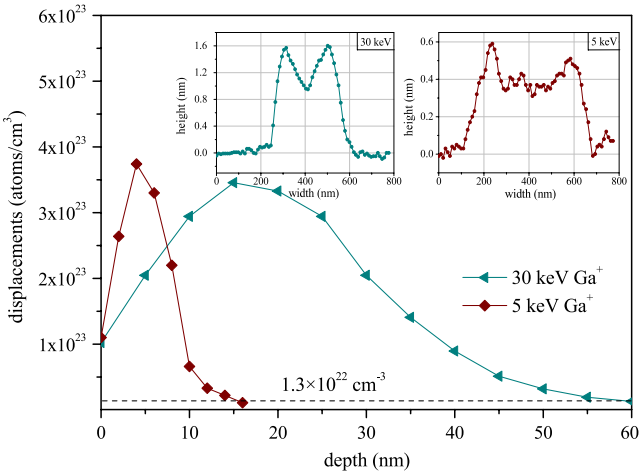

Figure 4. Atomic displacement distribution (Si recoils) as calculated by SRIM using 491 ions for 30 keV and 2.4 × 10^4 ions for 5 keV. The critical atom displacement concentration for the crystalline-to-amorphous transition is marked by the dashed line. The insets show two AFM profiles of the structures (300 nm in diameter) milled with the above-mentioned number of ions per milling point (which represents the initial stages of milled holes presented in figure 1).

X is the percentage of scattered ions from the wall and Y_s is the sputtering yield. Using the beam parameters given in table 1, for the 5 μs dwell time and 20 nm deep hole we obtain $N = 196$ for 5 keV ions and $N = 799$ for 30 keV. Since at 5 keV the number of passes to sputter the same depth in comparison to 30 keV must be increased ∼10 times, we get $N \approx 1960$ at 5 keV. For deeper holes the number of sputtered atoms from the hole bottom becomes the same for 5 and 30 keV ions due to the increasing number of 30 keV ions scattered towards the hole bottom (see figures 3(b) and (c)).

3.3. Surface swelling

The smaller ion range for low energy ions has further consequences. For instance, it is known that the surface swelling of silicon occurring after ion irradiation with a sufficiently small fluence is caused by amorphization of the irradiated volume [28, 29]. Since the crystalline silicon has larger density than the amorphous one and the sputtering is insignificant at low fluence, the amorphized region increases its volume, resulting in a small (several nanometres) surface protrusion. This effect is responsible for a small rim around the milled structures being visible also in figure 1(a). The amorphized volume can be estimated from SRIM-calculated recoil distributions. The dependence of atom displacements on the target depth is shown in figure 4 for 30 and 5 keV ions. To compare the theoretical results with the experimental data we did milling with a very low ion fluence, where each milling point of a circular hole (300 nm in diameter) is exposed by the same number of ions as used in the SRIM simulations (491 ions for 30 keV, 2.4 × 10^4 ions for 5 keV). The two insets in figure 4 show the surface profiles measured by AFM. The maximum protrusion height is 1.6 nm and 0.6 nm for 30 keV and 5 keV, respectively. According to [30], the critical atom displacement

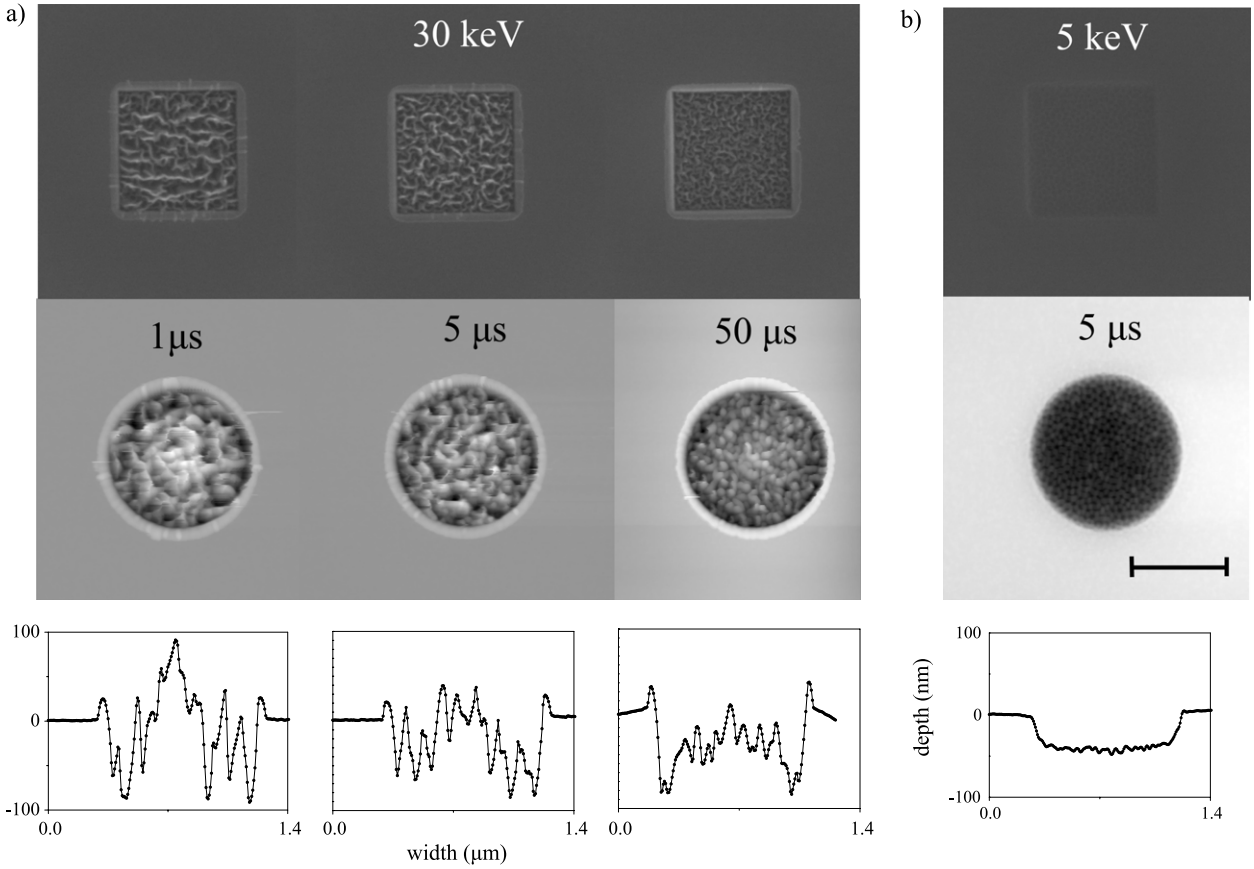

Figure 5. Patterning of a Ge (100) wafer. Top row: SEM images, middle row: AFM images, bottom row: AFM profiles measured on circular holes. (a) Holes milled by 30 keV ions using indicated dwell times. (b) Holes milled by 5 keV ions. The scale bar is 500 nm long.

concentration for a crystalline-to-amorphous transition in Si is $\sim 1.3 \times 10^{22}$ cm^{-3}. This concentration is marked in the image and the corresponding depth of the amorphous region is 58 nm and 16 nm for 30 keV and 5 keV, respectively. Since the amorphous layer density is 93% of the crystalline one [31], the theoretical protrusion height is 1.4 nm and 0.4 nm for 30 keV and 5 keV, respectively, which is close to the values obtained experimentally. The deviation from the experimental data is due to the finite size of the beam (the amorphized area is larger), while in the simulation all the ions are incident at a single point. Also note that for the holes deeper than $\sim$16 nm and milled with 5 keV ions the rim vanishes due to sputtering by the extended beam tails.

4. Germanium milling

Germanium is known to form nanoporous structures if irradiated with high energy ions (100 keV Ga^+ ions [32], 300 keV Ge^+ ions [33]). This obviously represents a challenge for patterning germanium by FIB at the nanoscale. The example of fabrication of germanium nanostructures having 1 μm lateral dimensions using 30 keV Ga^+ ions is shown in figure 5(a). The appearance of smaller structures (300 nm) was very similar: for clarity, only 1 μm structures are presented. The patterning parameters for 300 nm structures were the same as for those milled into silicon, presented in figure 1 (see table 2(a) and (b)). For larger structures the loop time was increased due to the larger number of milling points; dwell time and number of passes remain the same. Due to the higher sputtering yield of germanium in comparison to silicon (see table 1) the depth of the milled structures was expected to be accordingly higher (48 nm for 30 keV ions, 42 nm for 5 keV ions, based on SRIM-calculated sputtering yield in table 1). Instead of holes very large porous structures were created with protrusions reaching out above the initial surface up to 100 nm. The sputtering became more significant after applying a larger beam dwell time of 50 μs. A further increase of the dwell time led to no major change since the milled profile was deformed due to enhanced sputtering on inclined local surfaces in the same way as shown for silicon in figure 1(c). If the ion beam energy is decreased, the milling becomes more uniform than for 30 keV and again independent of the dwell time as in the case of silicon. The hole milled with 5 keV ions is 40 nm deep and the bottom is still porous, but smoother as determined by AFM (30 keV: RMS = 30.3 nm; 5 keV: RMS = 3.7 nm).

The morphology of the germanium surface hit by Ga^+ ions is ruled by two processes—formation of nanopores and growth of protrusions above the original surface. The nanopore formation is caused by the generation of point defects in the sample due to ion irradiation. The number of vacancies can be estimated by SRIM (see table 1). The value is significantly lower for 5 keV ions than for 30 keV ones. If the vacancies are mobile enough, they accumulate to form voids below the

surface [34]. These voids, once uncovered by the incident ion beam, cause the sputtering to be highly inhomogeneous, finally resulting in the formation of nanopores. Hence, nanopore formation might be effectively lowered using low energy ions, which is apparently the result of our experiment.

The growth of protrusions above the original surface, as observed in our experiments with 30 keV ions, is, however, a more complex process. The explanation proposed here is therefore only speculative. The large dimensions of protrusions (up to 100 nm) indicate that the swelling of the surface due to differences in density between crystalline and amorphous phases (similar to silicon) cannot be used as a proper explanation. Based on molecular dynamics modelling, Mayr and Averback [35] showed that strong stresses are generated in ion-bombarded germanium, which can be released by a swelling of the amorphous surface layer in the direction normal to the surface. The amount of stress correlates with the number of vacancies formed (see table 1). Therefore, lowering the ion energy reduces the stress amount in the surface layer and, subsequently, the height of the swelled surface.

5. Conclusions

Shallow nanostructures were milled by FIB into silicon and germanium substrates in order to investigate the influence of the Ga ion beam and its scanning parameters onto nanostructure shapes. For fabrication of silicon nanostructures it is beneficial to use low energy ions (<5 keV) as the current density of a low energy ion beam is significantly lower than the one provided by conventional 30 keV ions (even for the smallest beam currents). By applying low energy ions many scanning artefacts can be suppressed while keeping a large number of scanning loops. For instance, redeposition and enhanced sputtering at inclined surfaces are very effectively reduced.

Low energy ions are also more beneficial for milling germanium wafers as the application of a 30 keV ion beam tends to form nanoporous structures. Smaller numbers of ion-induced vacancies, as well as lower energy delivered to the sample by low energy ions, help to keep the milling process optimal and still efficient for both materials studied, although they behave differently upon ion irradiation (amorphization of silicon versus nanopore formation in germanium).

However, for applications requiring a superior resolution it would be necessary to use a protective layer at low energies to suppress the sputtering resulting from extended beam tails. It has also been shown that the ion scattering from walls (so-called self-focusing) becomes effective only if the milled feature depth is large enough; for shallow structures it can be neglected.

Acknowledgments

This work was supported by the research programmes of the Ministry of Education of the Czech Republic (project nos. MSM0021630508 and LC06040), GAAV (project no. KAN400100701) and the EUROCORES-GACR (project no. FON/06/E001). MK acknowledges the support of MSMT (2E08017) and FEI Company.

References

[1] Li W-H, Kang D-J, Blamire M G and Huck W T S 2003 *Nanotechnology* **14** 220
[2] Wanzenboeck H D, Waid S, Bertagnolli E, Muehlberger M, Bergmair I and Schoeftner R 2009 *J. Vac. Sci. Technol.* B **27** 2679
[3] Nellen P M, Callegari W and Brönnimann R 2006 *Microelectron. Eng.* **83** 1805
[4] Wilhelmi O, Reyntjens S, Mitterbauer C, Roussel L, Stokes D J and Hubert D W H 2008 *Japan. J. Appl. Phys.* **47** 5010
[5] Hopman W C L, Ay F, Hu W, Gadgil V J, Kuipers L, Pollnau M and de Ridder R M 2007 *Nanotechnology* **18** 195305
[6] Tsai C-H, Liao L-D, Luo Y-S, Chao P C-P, Chen E-C, Meng H-F, Chen W-D, Lin S-K and Lin C-T 2010 *Microelectron. Eng.* **87** 1331
[7] Lehrer C, Frey L, Petersen S, Ryssel H, Schäfer M and Sulzbach T 2004 *J. Vac. Sci. Technol.* B **22** 1402
[8] Karmous A, Berbezier I and Ronda A 2006 *Phys. Rev.* B **73** 075323
[9] Gherasimova M, Hull R, Reuter M C and Ross F M 2008 *Appl. Phys. Lett.* **93** 023106
[10] Lee J Y, Nordhoek M J, Smereka P, McKay H and Millunchick J M 2009 *Nanotechnology* **20** 285305
[11] Portavoce A, Kammler M, Hull R, Reuter M C and Ross F M 2006 *Nanotechnology* **17** 4451
[12] Čechal J, Tomanec O, Škoda D, Koňáková K, Hrnčíř T, Mach J, Kolíbal M and Šikola T 2009 *J. Appl. Phys.* **105** 084314
[13] Imre A, Ocola L E, Rich L and Klingfus J 2010 *J. Vac. Sci. Technol.* B **28** 304
[14] Kato N I 2004 *J. Electron. Microsc.* **53** 451
[15] Bals S, Tirry W, Geurts R, Yang Z and Schryvers D 2007 *Microsc. Microanal.* **13** 80
[16] Ziegler J F, Ziegler M D and Biersack J P 2010 *Nucl. Instrum. Phys. Res.* B **268** 1818
[17] Moberly Chan W J 2009 *J. Phys.: Condens. Matter* **21** 224013
[18] Hayat A, Berkovitch N and Orenstein M 2009 *Appl. Phys. Lett.* **94** 063103
[19] Kim H-B, Hobler G, Steiger A, Lugstein A and Bertagnolli E 2007 *Nanotechnology* **18** 245303
[20] Kim H-B, Hobler G, Steiger A, Lugstein A and Bertagnolli E 2007 *Nanotechnology* **18** 265307
[21] Adams D P and Vasile M J 2006 *J. Vac. Sci. Technol.* B **24** 836
[22] Prenitzer B I, Urbanik-Shannon C A, Gianuzzi L A, Brown S R, Irwin R B, Shofner T L and Stevie F A 2003 *Microsc. Microanal.* **9** 216
[23] Frey L, Lehrer C and Ryssel H 2003 *Appl. Phys.* A **76** 1017
[24] Platzgummer E *et al* 2006 *Microelectron. Eng.* **83** 936
[25] Beuer S, Rommel M, Lehrer C, Platzgummer E, Kvasnica S, Bauer A J and Ryssel H 2007 *Microelecron. Eng.* **84** 810
[26] Tripathi S K, Shukla N, Rajput N S and Kulkarni V N 2009 *Nanotechnology* **20** 275301
[27] Tripathi S K, Shukla N and Kulkarni V N 2009 *Nanotechnology* **20** 075304
[28] Huey B D and Langford R M 2003 *Nanotechnology* **14** 409
[29] Lugstein A, Basnar B, Hobler G and Bertagnolli E 2002 *J. Appl. Phys.* **92** 4037
[30] Menzel R, Gärtner K, Wesch W and Hobert H 2000 *J. Appl. Phys.* **88** 5658
[31] Wang J B, Datta A and Wang Y L 1998 *Appl. Surf. Sci.* **135** 129
[32] Yanagisawa J, Takarabe K, Ogushi K, Gamo K and Akasaka Y 2007 *J. Phys.: Condens. Matter* **19** 445002
[33] Romano L, Impellizzeri G, Tomasello M V, Giannazzo F, Spinella C and Grimaldi M G 2010 *J. Appl. Phys.* **107** 084314
[34] Holland O W, Appleton B R and Narayan J 1983 *J. Appl. Phys.* **54** 2295
[35] Mayr S G and Averback R S 2005 *Phys. Rev.* B **71** 134102